# Telecom-band coherent perfect absorption and asymmetric interferometric light–light control in a borophene–dielectric nanostructure

JinRong Liu,[a,b] XinHua Liao,[a,b] Qi Lin,[a] Xiang Zhai,[c] and Gui-Dong Liu,[a, c*]

a. *School of Physics and Optoelectronics, Xiangtan University, Xiangtan 411105, China. E-mail: gdliu@xtu.edu.cn*
b. *Hunan Key Laboratory for Computation and Simulation in Science and Engineering, Xiangtan University, Hunan 411105, China.*
c. *School of Physics and Electronics, Hunan University, Changsha 410082, China.*

## Complex surface conductivities of borophene

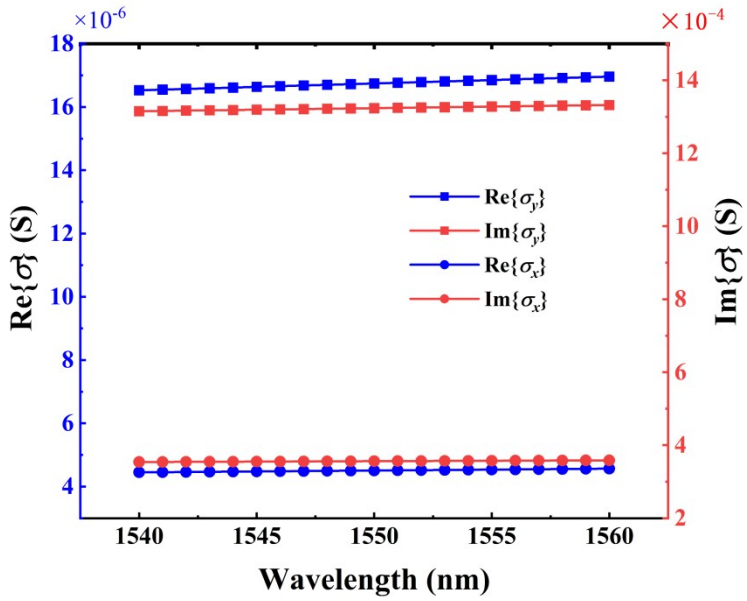


**Fig. S1.** Wavelength-dependent complex surface conductivities of borophene used in the simulations. The square and circle symbols denote the optical responses along the *y*- and *x*-directions, respectively. The left and right axes correspond to the real and imaginary parts of the surface conductivity, respectively.

To further clarify the anisotropic optical parameters of borophene used in the simulations, wavelength-dependent complex surface conductivities along the *x*- and *y*-directions are provided in this section.

In the FDTD simulations, borophene is treated as an anisotropic two-dimensional conducting sheet located at the interface between the dielectric grating and the dielectric slab, rather than a finite-thickness bulk medium. Therefore, the optical response of borophene is introduced through the in-plane complex surface conductivities $\sigma_x$ and $\sigma_y$, which are the actual material parameters implemented in the simulations.

The surface conductivities are calculated using the Drude-type conductivity model and parameters defined in the main text. The calculated complex surface conductivities are shown in Fig. S1. Since $m_y < m_x$, the Drude weight along the *y*-direction is larger than that along the *x*-direction. As a result, both the real and imaginary parts of $\sigma_y$ are larger than those of $\sigma_x$ in the investigated wavelength range. These anisotropic surface conductivities directly determine the direction-dependent optical response of borophene used in the FDTD model.

For an atomically thin two-dimensional material, an equivalent bulk dielectric function can be introduced only after assigning an effective thickness. Since this effective thickness is model-dependent, the complex surface conductivity is presented here as the primary optical parameter, providing a direct description of the borophene response used in the simulations.

## Evidence of guided-mode resonance

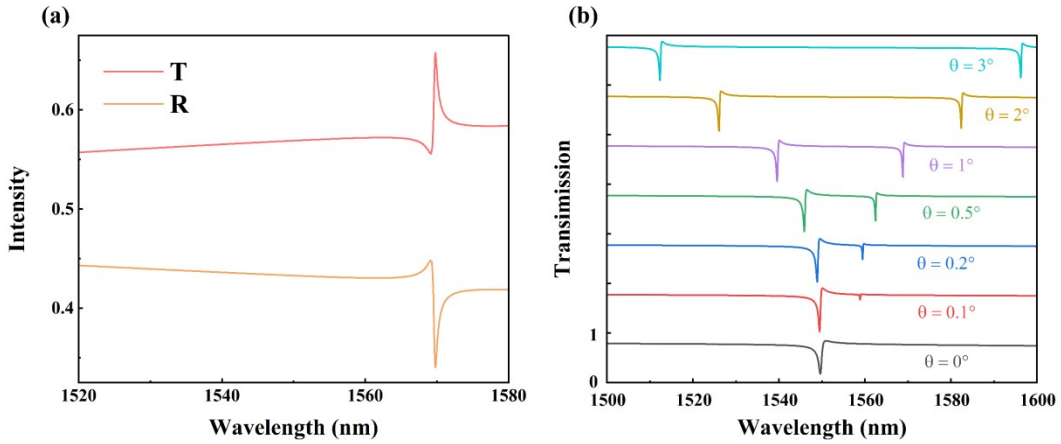


**Fig. S2.** Evidence of guided-mode resonance. (a) Transmission and reflection spectra of the dielectric grating-waveguide structure without the borophene layer. (b) Transmission spectra at different incident angles under single-side TE-polarized illumination from the upper port. The spectra in (b) are vertically shifted for clarity.

To verify the guided-mode-resonance origin of the resonant field localization discussed in Fig. 3(b) of the main text, we performed two additional simulations, as shown in Fig. S2.

First, the borophene layer was removed from the structure, and the reflection and transmission spectra of the remaining dielectric grating-waveguide structure were calculated. As shown in Fig. S2(a), a sharp resonant feature appears near the operating wavelength. Since borophene is absent in this simulation, this resonance cannot originate from the material absorption of borophene. Instead, it is supported by the dielectric grating-waveguide structure itself, indicating the existence of a leaky guided resonance.

Second, we calculated the angle-dependent transmission spectra of the complete structure with the borophene layer under single-side TE-polarized illumination from the upper port. These simulations are not intended to demonstrate CPA directly, but to identify the modal origin of the resonance that supports the CPA response. For a one-dimensional grating-waveguide structure, the excitation of a guided-mode resonance is governed by the in-plane phase-matching condition[39]

$$\beta(\omega) = \left| k_{\parallel} + mG \right|, \qquad \text{* MERGEFORMAT (S1)}$$

Where $\beta(\omega)$ is the propagation constant of the guided mode, $k_{\parallel} = k_0 \sin\theta$ is the in-plane wave vector of the incident light along the grating periodic direction, $k_0 = 2\pi/\lambda$ is the free-space wave vector, $\theta$ is the incident angle, $m$ is the diffraction order, and $G = 2\pi/P$ is the reciprocal lattice vector of the grating.

The grating-coupled guided mode can propagate in two opposite directions along the periodic direction. Therefore, under oblique incidence, the corresponding phase-matching conditions can be written as

$$\beta_{\pm}(\omega) = \left| mG \pm k_0 \sin\theta \right|. \qquad \text{* MERGEFORMAT (S2)}$$

At normal incidence, $k_{\parallel} = 0$, and the two counter-propagating guided modes satisfy the same phase-matching condition. Thus, only one resonance appears in the transmission spectrum. When $\theta \neq 0°$, the in-plane wave vector $k_{\parallel}$ breaks this equivalence, and the two counter-propagating guided modes satisfy different phase-matching conditions. Consequently, the original resonance splits into two branches. The separation between the two branches increases with $\theta$, because the difference between the two required propagation constants scales approximately as $2k_0 \sin\theta$.

As shown in Fig. S2(b), a single resonance dip is observed at normal incidence, whereas two separated dips appear and move apart as the incident angle increases. One branch shifts toward shorter wavelengths and the other toward longer wavelengths, consistent with the two phase-matching conditions in Eq. (S2). This angle-induced splitting is a typical signature of guided-mode resonance and supports that the resonance responsible for the CPA response is a grating-coupled guided mode. In the complete structure, this guided-mode resonance enhances the local field near the borophene layer, while borophene provides the intrinsic dissipation channel required for coherent perfect absorption.

## Fabrication tolerance analysis for slab thickness and grating width

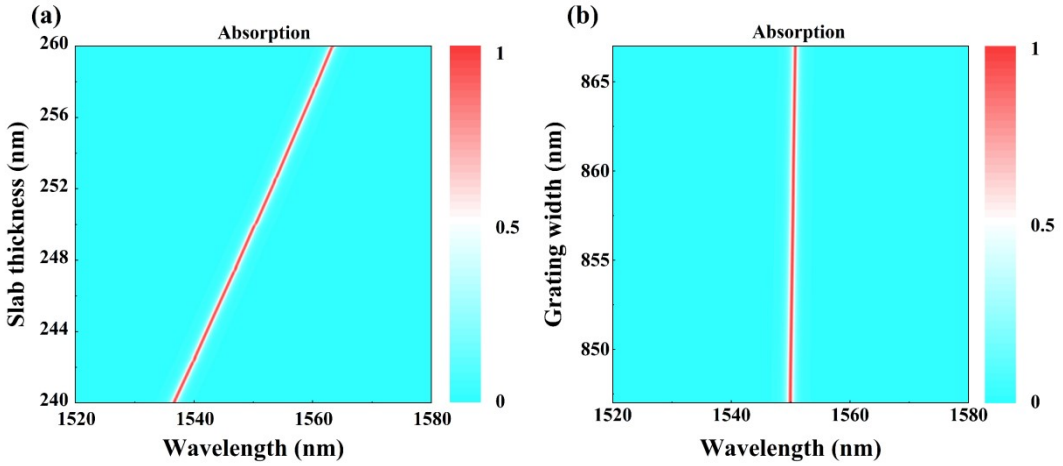


**Fig. S3.** Absorption spectra as functions of wavelength under variations of structural parameters: (a) slab thickness *t*, and (b) grating width *w*.

To further evaluate the fabrication tolerance of the proposed coherent perfect absorber, we additionally investigate the influence of slab thickness *t* and grating width *w* on the coherent absorption response. The corresponding two-dimensional absorption maps are shown in Fig. S3.

As shown in Fig. S3(a), when the slab thickness *t* increases from 240 nm to 260 nm, the high-absorption resonance exhibits a clear redshift along the wavelength axis. This behavior indicates that the slab thickness mainly modifies the optical path length and the effective phase-matching condition of the guided-mode resonance. Importantly, the near-unity absorption feature is maintained over the investigated thickness range, suggesting that moderate deviations in the slab thickness do not destroy the CPA response but mainly shift the operating wavelength. Fig. S3(b) shows the absorption map as a function of the grating width *w*. Compared with the slab thickness, the grating width has a much weaker influence on the resonance wavelength. The high-absorption peak remains nearly fixed around the designed operating wavelength, and the absorption intensity is preserved over the investigated range. This result indicates that the proposed structure has good tolerance to grating-width variations, which is beneficial for practical nanofabrication.

Together with the parameter scans of the grating period *P* and grating height *h* shown in Fig. 4 of the main text, these results confirm that the CPA behavior is not restricted to a single exact geometry. Reasonable deviations in key structural parameters mainly lead to predictable resonance shifts, while the high-absorption response can still be maintained.

## Angular sensitivity of the guided-mode resonance

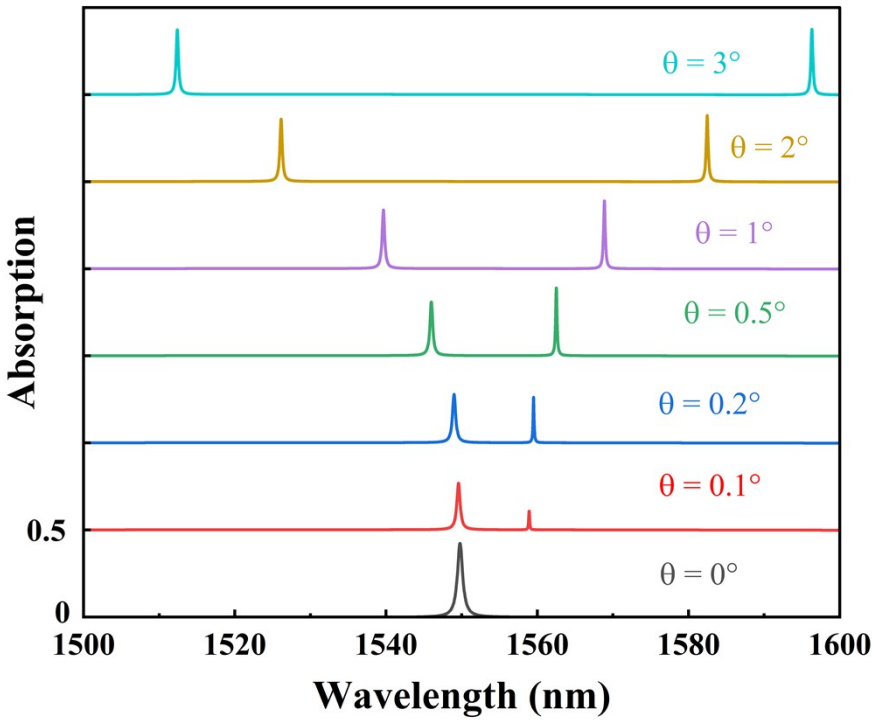


**Fig. S4.** Single-port oblique-incidence absorption spectra of the proposed borophene–dielectric nanostructure under TE-polarized illumination. The incident angle θ is varied from 0° to 3°.

To further evaluate the influence of angular deviation on the resonant response, we calculated the absorption spectra of the proposed structure under single-port oblique incidence. The incident light is TE-polarized, and the incident angle θ is varied from 0° to 3°. As shown in Fig. S4, a single resonance peak appears at normal incidence. When the incident angle becomes nonzero, the resonance splits into two branches. With increasing θ, one branch shifts toward shorter wavelengths, whereas the other branch shifts toward longer wavelengths, and the spectral separation between the two branches increases gradually.

This behavior is a typical signature of guided-mode resonance in a one-dimensional grating-waveguide structure. The angular splitting can be understood from the grating-assisted phase-matching condition. At normal incidence, the in-plane wave vector is zero, and the two counter-propagating guided modes satisfy the same phase-matching condition. Therefore, they are degenerate and appear as a single resonance. Under oblique incidence, the finite in-plane wave vector $k_{||} = k_0 \sin\theta$ breaks this degeneracy. The two counter-propagating guided modes then satisfy different phase-matching conditions, resulting in two separated resonant branches.

Although these simulations are performed under single-port excitation and are not intended to directly demonstrate dual-port non-collinear CPA, they reveal that the guided-mode resonance supporting the CPA response is sensitive to angular deviation. Therefore, in a practical two-port CPA configuration, non-collinearity between the two incident beams is expected to perturb the destructive-interference condition and reduce the CPA contrast. Accurate beam alignment and phase-front matching are therefore important for achieving ideal coherent perfect absorption.

**Reference**

39 Y.-X. Zhang, Q. Lin, X.-Q. Yan, L.-L. Wang and G.-D. Liu, Opt. Express, 2024, 32, 10669–10682.